JCI The Journal of Clinical Investigation

B cells, antibody-secreting cells and virus-specific antibodies respond to herpes simplex virus-2 reactivation in skin

Emily S. Ford, Anton M. Sholukh, RuthMabel Boytz, Savanna S. Carmack, Alexis Klock, Khamsone Phasouk, Danica Shao, Raabya Rossenkhan, Paul T. Edlefsen, Tao Peng, Christine Johnston, Anna Wald, Jia Zhu, Lawrence Corey

J Clin Invest. 2021. https://doi.org/10.1172/JCI142088.

Research In-Press Preview **Immunology** **Infectious disease**

Graphical abstract

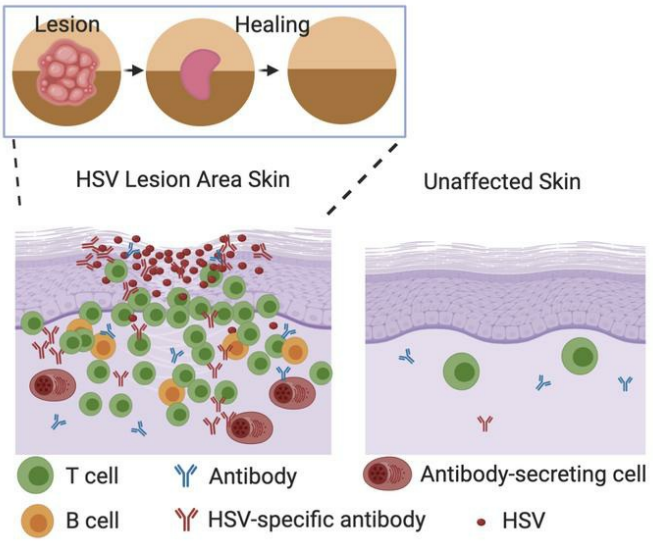

B cells, antibody-secreting cells and virus-specific antibodies respond to herpes simplex virus-2 reactivation in skin

Emily S. Ford*[1,2], Anton M. Sholukh*[1], RuthMabel Boytz[1], Savanna S. Carmack[3], Alexis Klock[3], Khamsone Phasouk[1], Danica Shao[1], Raabya Rossenkhan[1], Paul T. Edlefsen[1], Tao Peng[1,3], Christine Johnston[1,2], Anna Wald[1,2,3,4], Jia Zhu[1,3] and Lawrence Corey[1,2,3,§]

*These authors contributed equally to this work

[§]Corresponding Author:

Lawrence Corey, 1100 Eastlake Avenue E. E3-110, Seattle, WA 98109, Phone 206-667-6770, email lcorey@fredhutch.org

Affiliations:
[1]Vaccine and Infectious Diseases Division, Fred Hutch Cancer Research Center, Seattle WA, USA
[2]Division of Allergy and Infectious Diseases, Department of Medicine, University of Washington, Seattle WA, USA
[3]Department of Laboratory Medicine and Pathology, University of Washington, Seattle WA
[4]Department of Epidemiology, University of Washington, Seattle WA

Conflict of Interest:
The authors have declared that no conflict of interest exists.

Funding Sources:
NIH: K08 AI148588 (ESF), U19 AI113173 (ESF), P01 AI030731 (JZ, LC, AW), R01 AI042528 (JZ, LC), R01 AI134878 (JZ, LC), P30 CA015704 (core facilities), VIDD Initiative grant (AMS)

Abstract

Tissue-based T cells are important effectors in the prevention and control of mucosal viral infections – less is known about tissue-based B cells. We demonstrate that B cells and antibody-secreting cells (ASCs) are present in inflammatory infiltrates in skin biopsies of persons during symptomatic HSV2 reactivation and early healing. Both $CD20^+$ B cells, most of which are antigen-inexperienced by co-expression of IgD, and ASCs, characterized by dense IgG RNA expression in combination with CD138, IRF4 and Blimp1 RNA, are seen to colocalize with T cells. ASCs are found clustered with $CD4^+$ T cells, suggesting potential for crosstalk. HSV2-specific antibodies to virus surface antigens are also present in tissue and increase in concentration during HSV2 reactivation and healing, unlike in serum where concentrations remain static over time. B cells, ASCs, and HSV-specific antibody were rarely detected in biopsies of unaffected skin. Evaluation of serial biopsies demonstrate that B cells and ASCs follow a more migratory than resident pattern of infiltration in HSV-affected genital skin, in contrast to T cells. Together, these observations suggest distinct phenotypes of B cells in HSV-affected tissue; dissecting their role in reactivation may reveal new therapeutic avenues to control these infections.

Introduction

In immunocompetent hosts, after initial exposure at the site of non-intact epithelialized skin or mucosa, herpes simplex virus 2 (HSV2) establishes chronic latent infection of the associated dorsal root ganglion (1, 2). The spectrum of clinical disease among infected persons is broad; some experience asymptomatic seroconversion while others have 10 or more recurrences a year. While the mechanisms underlying viral reactivation and symptomatic disease are not

known, the spectrum of clinical manifestations at the site of reactivation is thought to depend primarily on the host adaptive immune response, rather than intrinsic viral factors (3, 4). As suggested by human-based studies and supported by mathematical modeling and animal studies, cell-mediated immunity, including tissue-resident memory $CD8^+$ and infiltrating or resident memory $CD4^+$ T cells are important factors in local viral control (5–10).

The role of humoral immunity in the human response to HSV2 reactivation is less clear. Robust titers of binding and neutralizing antibodies are commonly detected in the blood, but are not associated with the frequency of HSV2 symptoms in natural infection (11, 12) or after vaccination (13–15). Vaccine-induced antibody to gD was not protective against primary infection in HSV2-seronegative persons (16). One proposed theory is that a dominant antigen, gD, leads to the production of antibodies that are binding and neutralizing, but not protective (17). Other theories include that certain HSV-specific antibodies may function protectively in tissue near the site of viral release but circulating antibody levels do not reflect this tissue-based event (18), or that cell-to-cell spread of virus is sufficient for propagation and development of symptomatic reactivation even in the presence of effective neutralizing antibodies, but the concentration of such antibodies is below the threshold of efficacy (19).

Some evidence from animal models suggest that B cells are important to protection from HSV2. B cell-deficient mice rapidly develop severe disease after HSV2 genital challenge (6, 20), and this effect is limited if B cells are depleted after immunity has been developed (21) suggesting that at least part of the role of B cells is in the primary immune response. Whether anti-viral

activity is related to systemic or local secretion of antibody is an area of active investigation. In a guinea pig HSV2 infection model where recurrences have been observed, ASCs have only been seen in secondary lymphoid and neuronal tissues (22, 23), and systemically-infused antibody rescued control of HSV2 shedding in B-cell depleted animals (21). In HSV2-exposed mice, however, B cells (both $CD20^+$ and $CD138^+$ IgG^+) infiltrate into the vaginal mucosa in response to immunization and rechallenge with latency-deficient HSV2. These B cells are associated with intraluminal vaginal secretion of HSV-specific IgG2 and IgA during viral challenge, but not at other times (24). In concert with the discovery of memory lymphoid clusters in mice infected with HSV2, these recent observations have raised the possibility that B cells and ASCs may function outside of their previously understood role in lymph tissue. In humans, the role of B cells during HSV2 infection has not been studied. From single cell dissociation studies, B cells are identified in normal skin, but are very rare (25, 26). With histologic confirmation of their presence in the tissue extrinsic to blood vessels, antibody-secreting cells (ASCs) are identified in human foreskin (27). B cells have been observed, albeit infrequently, in inflammatory infiltrates related to HSV (28), and their presence in the skin has been confirmed by single-cell and RNAseq technology (26, 29, 30). Whether B cells and ASCs are actively involved during the immune response to HSV2-reactivation in humans in non-mucosal skin, therefore, is unknown.

We utilized our repository of sequential genital skin biopsies from persons with HSV2 to explore whether B cells and ASCs are present in genital skin biopsies taken during HSV2 reactivation and clinical quiescence. HSV2-specific antibody is present in tissue and the concentration varies

over time suggesting the possibility of local antibody production. In a time of rapidly-expanding information from single-cell dissociation studies, this histologic information confirms the importance of spatially-informative methods, and urges further investigation into the role of B cells and ASCs in local inflammatory processes.

Results

Of 16 participants, 14 were women; the median age was 50 years (range 18-66). All 16 were seropositive for HSV2 and 6 also had antibody to HSV1. The most common site of biopsies was the buttock (N=10) (**Supplementary Table 1**). Biopsies were performed during a clinically evident HSV2 lesion and during healing, for a total of 5 or 6 biopsies per person. A control site biopsy of uninvolved skin was performed at the time of the lesion or 8 weeks after healing from either the arm (N=7) or the contralateral genital skin (N=9). There were no complications associated with serial biopsies (5, 8).

Histology of B cells in tissue by immunofluorescence

B cells were identified by dual immunofluorescent staining of CD20 and CD79b in 47 of 65 punch biopsies of active and early healing HSV2 lesions from 11 persons where complete sets of 5 or 6 biopsies from the active lesion to 8 weeks after healing were available for IF. Per person, a median of 5 of 6 biopsies were seen to have B cells (range 2-6 of 6); in most persons B cells were present in all of the biopsies from the HSV2 lesion site. In 3 persons, 10 or fewer B cells were seen in any of the biopsies, but $CD20^{+}CD79b^{+}$ B cells were seen in at least two of the biopsies from all persons. CD20 and CD79b were chosen for IF due to their relative abundance

on the B-cell surface (CD20 is expressed at 6-fold higher density than CD19 (31)) and consistent performance in this assay. To confirm the identity of these cells and minimize the risk of non-specific antibody binding, dual staining was employed initially. After quantification and confirmation of CD20 reliability by dual staining, CD20 was used independently to identify B cells in tissue biopsies. The number of $CD20^{+}CD79b^{+}$ cells present in each biopsy section varied by person and timepoint. In general, B cells were more common during the lesion and early healing, similarly to T-cell infiltration (5). They were infrequent in biopsies during clinical quiescence (present in only 3 of 11 biopsies taken at 8 weeks post healing) and were detected in only 3 of 16 control site biopsies either from uninvolved genital skin or the arm (**Figure 1A**).

Histologically, B cells were identified by CD20 IF in the upper dermis (typically within 500 μm of the surface epithelium) and were never found within the dermal-epidermal junction (DEJ) (**Figure 1A**), where $CD8^{+}$ T cells are often found (**Figure 1B**) (5), or the multiple layers of the epidermis, consistent with histology in mice (32). $CD20^{+}CD79b^{+}$ cells were most often observed to be distributed within areas of immune cell infiltration (as in the healing biopsy in **Figure 1A**) but were also identified similarly located in dense groups of T cells by staining of serial sections (**Figure 1C**), suggesting in vivo interactions between the two subpopulations of cells. T cells are often observed to be present near hair follicles or skin-localized glandular structures and this was likewise occasionally observed of B cells. CD27, a canonical marker of memory B cells, is more strongly expressed by activated T cells and thus is abundant in skin biopsies during HSV2 reactivation and healing. Co-staining of this marker may therefore be unreliable in biopsies with robust T-cell infiltration, but in B-cell containing biopsies from 5 individuals little to no overlap

in staining of CD20 and CD27 was observed in B cells, suggesting that the majority of observed $CD20^+$ cells are not memory B cells (**Figure 1D**).

To determine whether these $CD20^+CD27^-$ cells could instead represent a naïve or antigen-unexperienced population, IgD co-staining by IF was performed in biopsies from 5 persons. $CD20^+IgD^+$ double positive cells were seen in all 5 persons (representative image with dual color images shown in **Figure 1E**). In one person, nearly all $CD20^+$ cells were also IgD^+, however in other persons there was more variability and some $CD20^+$ cells were observed not to have IgD^+ co-staining. We suspect that the majority of $CD20^+$ cells observed are indeed antigen-unexperienced and there may also be smaller populations of other B-cell phenotypes present.

To investigate the presence and distribution of antibody-secreting cells (ASCs), fluorescent in situ hybridization (FISH) directed at IgG RNA (pooled *IGHG1-4*) (ACD Bio) was performed to identify cells with dense expression of immunoglobulin transcripts. These cells were quantified in 57 biopsies from 10 persons. Both class-switched B cells and ASCs contain IgG mRNA, however, ASCs are known to express up to 1000-fold more immunoglobulin mRNA per cell than B cells (33, 34). High intensity, cytoplasmic, punctate fluorescence indicative of ASCs was observed in 48 of the 57 tested biopsies (**Figure 1F, 1G**). Histologically, these IgG RNA^+ cells followed tissue distribution patterns described above seen with $CD20^+$ B cells. No IgG RNA^+ cells were observed within the epithelial cell layers or in the DEJ in any biopsy. All IgG RNA^+ cells observed were present in the dermis. No IgG RNA^+ cells by FISH were identified in any of the control biopsies.

To further confirm the phenotype of ASCs in our tissue biopsies, we evaluated the presence of transcription factors Blimp-1 and IRF4 (35–37). Blimp-1 is encoded by the *PRDM1* gene. Evidence of both *PRDM1* and IgG RNA was detected in most but not all IgG RNA^{+} cells (**Figure 2A**). Further confirmation of the presence of ASCs was pursued by dual FISH with expression of transcriptional factor *IRF4* which is upregulated in ASCs by 5–10-fold compared to naïve and memory B cells (38) and also induces Blimp-1 expression (39). Nuclear *IRF4* production was frequently observed to be co-localized with IgG RNA transcripts by confocal microscopy (**Figure 2B, Supplementary Figure 3**). Taken together, these findings strongly indicate the presence of IgG-producing ASCs during HSV2 reactivation and skin healing. To further confirm this phenotype, co-expression of *MS4A1* (which encodes CD20) and *SDC1* (syndecan-1 or CD138) was also studied. *SDC1* is a canonical marker in flow cytometry and histology of ASCs (40, 41) but it is also highly expressed on the surface of epithelial cells including keratinocytes and is less abundant on other skin cells including endothelial cells and fibroblasts (42). Transcripts of *MS4A1* were visualized both with and without expression of IgG RNA, though more often these were seen independently (**Figure 2C**), and *SDC1* signal was observed in some, but not all cells expressing a high level of IgG RNA transcripts. Due to the abundant presence of *SDC1* in skin, deconvolution microscopy was used to confirm that *SDC1* and IgG RNA signal were concomitantly present in single cells. **Figure 2D** shows a single Z-stack image from these results, confirming that both *SDC1* and IgG RNA signals are coming from the same cells. These constellations of findings provide strong evidence that ASCs are selectively increased in tissue during the time of lesion and early healing periods of genital HSV reactivation. Likewise, it also

shows that ASCs of various stages of differentiation are present. The correlation between CD20 and IgG+ cells by repeated measures analysis was ~0.4, P=0.03 (see below).

To investigate whether we could use FISH to identify rare memory B cells, we chose *PAX5*, or B-cell-specific activator protein, a transcription factor that is expressed in naïve and memory lineage B cells but is downregulated by 4-5 fold in ASCs (38). Colocalization of a high level of *PAX5* with low level of IgG RNA would indicate a memory or antigen-experienced B cell. In genital skin biopsies from 5 individuals, we did not observe robust *PAX5* colocalization with IgG (**Figure 2E**). The overall frequency of *PAX5* detection was low, in 4 persons studied we did not observe any cells with dense *PAX5*/ IgG RNA co-expression, and *PAX5* signal was seen in cells not identified to have IgG transcription (potentially naïve B cells). This was confirmed with observation of consistent *PAX5* co-staining with *MS4A1* in 2 persons; all *MS4A1*$^{+}$ cells also expressed *PAX5* (**Figure 2E**). Minimal or no *PAX5* expression in cells containing a high level of IgG RNA transcripts supports that these cells are indeed ASCs.

While there are no validated markers to indicate tissue residence or migration of B cells, there is literature on B-cell migration from animal models and studies of autoimmunity (30, 32, 43, 44). CXCR4 is a known marker of plasma cell migration and retention in the bone marrow and is proposed to be important in plasmablast migration to sites of inflammation (44–47). Other chemokines, including CXCR3, CXCR5, and CCR7 have also been proposed (43). Here we saw evidence of *CXCR4* RNA expression in IgG mRNA-containing cells, suggesting that CXCR4 may contribute to the migration of ASCs in skin during HSV reactivation (**Figure 2F**). Evidence of

CXCR5 or CXCL13 expression was not seen. The primary ligand for CXCR4 (CXCL12) was observed in a gene expression study of HSV-infected tissue, but not significantly upregulated at healing or lesion time points (data accessible at NCBI GEO database (48, 49), accession GSE18527, **Supplemental Figure 1**).

We performed detailed studies of the spatial localization of B cells to define their proximity to small capillaries. Co-staining with von-Willenbrand Factor (vWF) indicated that IgG RNA$^+$ cells identified by FISH were, while at times near to small capillaries, were not typically contained within vascular structures (**Figure 3A**). Many clusters of IgG RNA$^+$ cells were observed that did not have evidence of associated endothelial cells (**Figure 1C, Figure 3B, 3C**). Some clusters appeared to contain primarily T cells, as in Figure 1D and as described previously (7, 8, 50), and others appeared to contain primarily ASCs, with a few T cells as in **Figure 3C**. Clusters of IgG RNA$^+$ cells were typically located in the dermis (not associated with the DEJ) and contained both CD8$^+$ (**Figure 3B**, by FISH and IF over serial sections) and CD4$^+$ (**Figure 3C,** by dual-probe FISH) T cells. Notably, these immune cell clusters have not been detected in any of the 27 control biopsies collected either from the arm or contralateral genital area. We also did not see any B cells or ASCs in vascular structures in control biopsies. Thus, dermal-infiltrating and capillary-associated B cells and ASCs are likely all related to HSV2 reactivation in genital skin.

Kinetics of B-cell response during HSV2 reactivation and skin healing

Overall, the magnitude and density of the B-cell and ASC infiltrate (**Figures 4A and B**) were greatest during the acute phases of reactivation; i.e., during clinical lesion and early healing.

HSV2 was detected by PCR at the time of lesion biopsy in 12 of 14 patients in whom this was tested, and in the first healing biopsy in patients 7 and 16. In most persons, the highest density of $CD20^+$ B cells was observed in biopsies when genital lesions were present; median density of 18.4 cells/mm^2 (N = 8, range 2.6 – 46.0 cells/mm^2). In three persons, the density of $CD20^+$ cells peaked at the time of healing, about 10 days after lesion onset (**Figure 4A**), with a median of 16.1 cells/mm^2 (range 1.5 – 37.4 cells/mm^2). To determine whether the peak density of $CD20^+$ B cells was higher at either active/early healing or later healing time points, the maximum of these biopsies for each person were compared. By Wilcoxon signed rank test, the maximum $CD20^+$ cell density of ulcerative or healing lesions was higher than the maximum of the 2, 4, or 8 weeks post healing biopsies ($p = 0.003$). In three persons (1, 7 and 10), few B cells were seen in any biopsies. This overall pattern of higher infiltration at the time of symptomatic disease is identical to the pattern observed in T cell infiltration (see below).

In three persons (4, 11 and 15), we noted an increase in IgG RNA^+ cells between the 4 and 8 weeks post-healing biopsies. Similarly, the $CD20^+$ B cell density increased at 8 weeks post healing in patients 2 and 13. We speculated that this could be related to subclinical viral reactivation, albeit proof of this was not present in any participant by HSV PCR from tissue. In contrast to $CD20^+$ B cells, by Wilcoxon signed rank test, the maximum IgG RNA^+ cell density of lesion or healing was no higher than the maximum of the 2, 4, or 8 weeks post healing biopsies ($p = 0.2$). In those three persons with a peak of IgG RNA^+ cells at 8 weeks post healing, the corresponding tissue antibody concentrations varied over time (4, 11, and 15); two had a peak

at the post-healing time and one peaked during the lesion, none of these persons had a corresponding peak in antibody titer at the 8 weeks post-healing time point.

The density of $CD20^+$ and IgG RNA^+ cells was considerably lower than the density of T cells at the site of HSV2 reactivation (**Figure 4C and 4D**). Similarly to past reports (8, 28), $CD4^+$ and $CD8^+$ T cells were found at highest density during a symptomatic lesion in the majority of persons. As with $CD20^+$ cells, by Wilcoxon signed rank test, the maximum $CD4^+$ and $CD8^+$ cell density of lesion or healing was higher than the maximum of the 2, 4, or 8 weeks post healing biopsies ($p = 0.008$, $p = 0.04$). We evaluated the relationship between B- and T-cell density in individual lesion biopsies (**Figure 4E**). Biopsies with the highest T-cell density tended to be those with higher B-cell density. By repeated measures correlation, there was a correlation between the number of $CD20^+$ B cells and CD4 and $CD8^+$ T cells, whereby biopsies with greater numbers of T cells also tended to have greater numbers of B cells, when accounting for multiple biopsy results per person. The repeated measures correlation coefficient (after log transformation) between $CD20^+$ cells and $CD4^+$ and $CD8^+$ T cell subsets was 0.64 (p 0.0002) and 0.77 ($p < 0.0001$). There was a small correlation between CD20 and IgG^+ cells by repeated measures correlation (r 0.40, $p = 0.03$). None of these correlations were as strong as the correlation between $CD4^+$ and $CD8^+$ T cells, where the correlation coefficient between $CD4^+$ and $CD8^+$ T cells was 0.83 ($p < 0.0001$) (**Figure 4E**). There was no correlation between IgG^+ cells and CD4 or $CD8^+$ T cells (r 0.28 and 0.31, p 0.33 and 0.28, respectively) **(Supplementary Figure 2).** The simultaneous migration and spatial clustering of T and B cells in genital skin during HSV2

reactivation and healing suggest that these lymphocyte subsets may be influenced by similar recruitment mechanisms.

Detection and kinetics of HSV2 specific antibodies in genital tissue

Antibody (IgG) was detectable by IF to human IgG in tissue. As with B cells, IgG was detected to the greatest extent in the upper dermis of lesion and early healing tissue biopsy sections and was less detectable in biopsies of uninvolved sites (**Figure 5A**). In a unique biopsy of an active HSV2 vesicle and areas of HSV2-associated epithelial cell necrosis, IgG was detectable co-localized with HSV antigen within the vesicle, and less prominent in the necrotic area (**Figure 5B**). Fluorescence was not detected with an isotype control, isolated secondary antibody or if the tissue was blocked with 5% human serum prior to IF (**Supplementary Figure 3**). We therefore hypothesize that IgG detected in skin during HSV2 reactivation (**Figure 5**) is produced by an antigen-specific process, such as by locally migrated B cells, and would thus be present at higher concentration than non-HSV-specific antibody.

We first investigated the trajectory of the systemic antibody response during HSV2 reactivation and healing via sequential serum samples from two persons collected concurrently with skin biopsies (all other participants had a single blood draw at study entry, which may not have occurred within 6 months of their biopsy series). We used an antibody binding assay based on the Luminex platform to detect antibodies specific to the major HSV2 surface glycoproteins gB2 and gD2. We included EBV gp350 and the stem of influenza hemagglutinin (Flu-HA) as highly prevalent, non-HSV targets. For all tested antigens, no variability in serum antibody level was

detected over time as evidenced by overlapping titration curves and the nearly identical values for the area under the curve (AUC) calculated for these titration curves (**Supplementary Figure 4** and **Supplementary Table 2**). This finding is consistent with earlier reports documenting the absence of systemic antibody response during local HSV2 reactivation (51–54).

To investigate whether immunoglobulin observed in biopsies by IF was specific to HSV2, we extracted immunoglobulin from sequential biopsies from 14 participants to measure IgG reactive to gB2, gD2, and total IgG. IgG reactive to gB2 and gD2 proteins was detectable in the majority of the lesion area biopsies but was not detected in many biopsies collected from the arm and contralateral skin (**Figure 6A, 6B**). When followed over time, the pattern of shifts in concentration of HSV-specific IgG (**Figure 6A, 6B**) and total IgG (**Figure 6C**) varied over time and by individual, similarly to B cells and ASCs. Over participants the amount of HSV-specific antibody varied by up to 30-fold. Within participants, the difference in the amount of HSV-specific antibody in different biopsies likewise varied substantially (gB2 median 3.4-fold, range 1.7 - 57.8, and gD2 median 6.1-fold, range 2.3 - 94.7). Some participants had a peak of HSV2 specific IgG at the lesion, others had a peak during early healing, and the rest showed a peak of HSV2-specific IgG at late healing. A higher concentration of total IgG was found at the lesion in biopsies from 6 participants and post-healing in 4 participants, the total amount of IgG in the control biopsies was generally low (**Figure 6C**). Conversely, there was no major change observed over the course of a lesion and healing in the levels of IgG specific to control antigens in skin extracts: EBV gp350 and Flu-HA (**Figure 6D**) except participant 6 for whom IgG at the

lesion was substantially higher than for subsequent time points. Antibodies to control antigens were observed in skin extracts of only a few persons.

We also used AUC of antibody titration curves to compare levels of circulating antibodies upon participant study intake. The amount of circulating antibody to gD2 was similar for the majority of the participants while the amount of gB2-specific IgG was more varied among participants (**Figure 6E, Supplementary Figure 5 and Table 3**). Both gB2 and gD2-specific IgG were present at significantly higher levels than IgG against non-HSV antigens, although the difference in levels between HSV2 antigens and EBV gp350 was less profound.

This discordance between antibodies to HSV-specific and control antigens in skin and serum also suggests in-tissue antibody production. While some of the discrepancy between control and HSV-specific antibody in tissue may be accounted for by its greater abundance in serum, that was not consistently true. For example, the level of EBV-gp350 IgG was similar to gB2 IgG in the serum of participant 13, whereas in skin EBV-gp350 IgG was not detected and gB2 IgG peaked at the healing time point (**Figure 6D**). In participant 8, EBV-gp350 IgG in serum was present at a higher level than gD2 and gB2-specific Abs, but in skin gD2 IgG peaked at 2 weeks post healing while EBV-gp350 IgG was increased at lesion time point. Interestingly, Flu-HA but not EBV IgG mirrored the dynamics of HSV-specific antibody in this participant. Together, these findings support multiple mechanisms of antibody infiltration into inflamed skin, including both transudation from serum and local production.

Discussion

Here we have shown that B cells of different developmental stages are present in biopsy tissue from persons undergoing biopsies of active and healing skin lesions caused by HSV2 reactivation. Our studies show B cells to be within the upper dermis and extrinsic to blood vessels in the weeks during and after HSV2 reactivation. Spatially, we see two intriguing patterns of B-cell infiltration. In the first, ASCs are present in the dermis at the site of HSV reactivation in variable density over time, and this coincides with the pattern of total immunoglobulin we see during genital lesions. The other pattern is the presence of largely antigen-inexperienced $CD20^+$ B cells in T-cell clusters and infiltrates. These B cells are primarily $CD20^+$ cells that co-express IgD but not memory markers and were not associated with Ig secretion by FISH staining; suggesting these are early-stage B cells that might participate in Ag processing or some as yet undefined function, such as regulation of inflammation. The robust correlation between B cells and CD4+ T cells corroborates this suggestion. Based on the finding of B cells in multiple stages of development in biopsies and closely organized within T cell clusters, we propose that B cells may be involved in antigen presentation and regulation of inflammation (55) as well as local production of antibody. This diversity of tissue B-cell subsets by spatiotemporal arrangement, phenotype, and a statistically significant but comparatively minor correlation between CD20 and IgG RNA also suggests that there is not a single mechanism of recruitment of different subsets of B cells. It is possible that tissue-infiltrating memory cells may give rise to ASCs during the course of HSV2 reactivation and healing, but with the paucity of detected memory cells, it appears more likely that there is an independent mechanism by which ASCs enter inflamed tissue. That B cells and ASCs are present at lower

numbers than T cells in the skin, as is true in the blood, is congruent with multiple, diverse roles in immune activation, regulation, or antibody production.

We have also found that HSV2-specific antibody extracted from skin biopsies varies in concentration over the course of reactivation and healing and is present at greater concentration than antibody unrelated to HSV antigens; whereas no variability is seen in serum over the same time intervals. The change in tissue antibody concentration corresponds to change seen in the density of ASCs, though they do not mirror each other directly. This is congruous with observations in other conditions where a peak in ASC density is offset in time to the peak in corresponding antibody production (56, 57). Overall, these findings are consistent with boosting of local antibody secretion by viral challenge whereby tissue-based antibody concentration is increased during HSV2-reactivation and healing, and much lower in uninvolved control tissues. The role of tissue-infiltrating antibody in control of viral replication during HSV-2 outbreaks has been suggested by mathematical and experimental models showing the importance of rapid suppression of cell-to-cell spread and neutralization of free virus during HSV-2 reactivation (4, 9). Further investigation to identify additional markers of tissue infiltration and recruitment of B cells is necessary; here we have observed scant CXCR4 in IgG RNA^+ cells but no CXCR5, CCR4 or CCR5 in B cells by IF in biopsy specimens (24). We suspect that there may be an antigen-dependent mechanism driving this process.

Mechanistic evaluation from human tissues is by necessity limited, and as such this study was limited in scope to those persons available and willing to undergo serial biopsies and blood

draws over the course of symptomatic HSV2 infection. This typically excludes those persons with mild disease (<1-2 outbreaks/year) and by definition excludes any persons who do not have symptomatic HSV outbreaks, who may have a very different local immune response.

In summary, we have demonstrated that B cells and ASCs are present in the inflammatory infiltrate that results from HSV2 reactivation in genital-region skin. Phenotypic testing indicates that the ASCs are for the most part plasma cells but this may include plasmablasts, and many, if not most $CD20^+$ cells seen are antigen-inexperienced. The kinetics of tissue infiltration and egress of $CD20^+$ cells, and less so IgG^+ cells, follows that seen in T-cell studies, though it varies by patient. This apparent variability may be partly due to the limited sample size available for study, however, it parallels the relative concentrations of HSV2-specific antibody. That the concentration of HSV2-specific antibody in tissue varies independently from the concentration of HSV2-specific antibody in serum suggests that there are local mechanisms either leading to local production or recruitment of HSV2-specific antibody. We propose an as of yet under-appreciated role of B cells and ASCs in the human skin-based immune response to HSV2 reactivation.

Methods

Study participants. Healthy, HSV2-seropositive adults with a history of symptomatic genital herpes were enrolled in a natural history biopsy protocol at the University of Washington Virology Research Clinic (UW-VRC) in Seattle, WA. Participants had symptoms of genital herpes for longer than 1 year and HSV2 seropositivity was confirmed by HSV Western blot (58).

Biopsies were performed by trained clinicians as described previously (5) at the time of an HSV2 lesion, at lesion healing 10–14 days after onset and in that same location 2, 4, and 8 weeks later. A control biopsy was obtained from the upper arm or contralateral genital region skin site. Blood for peripheral blood mononuclear cells (PBMC) and plasma isolation was drawn either at enrollment or at each biopsy visit for some study participants. The University of Washington Human Subjects Review Committee reviewed and approved the protocols and all participants provided written consent.

Materials. HSV2 proteins gB2 and gD2 were kindly provided by Drs. G.H. Cohen and R.J. Eisenberg, gD2 was also provided by Immune Design Inc. Epstein-Barr virus (EBV) gp350 was kindly provided by Dr. A. McGuire. Stem of influenza hemagglutinin (Flu-HA) strain H1 1999 NC was expressed using vector VRC-3925 (59) in 293F cell and was kindly provided by Drs. M. Gray and L. Stamatatos.

Immunofluorescence (IF): Biopsy specimens were flash frozen in optimum cutting temperature (OCT) compound (Sakura Finetek) and stored at −80 °C. Slices of tissue (8 μm) perpendicular to the epidermal surface, including a cross section of the epidermis, dermal-epidermal junction (DEJ), and dermis, were prepared by cryostat sectioning and mounted on glass slides. Slides were dehydrated at room temperature for 24 hours, frozen at -80°C, and fixed in acetone prior to use. To enumerate the relative density of B cells, T cells, ASCs, blood vessels and/or antibody in tissue biopsy sections, the following primary antibodies were used; rabbit anti–human CD20 (1:100; Abcam ab78237), mouse anti-human CD79b (1:100; Novus Biologicals NBP1-28528),

mouse anti-human IgG (1:100; eBioScience 05-4200), sheep anti-human von-Willenbrand Factor (vWF) (FITC-conjugated, 1:5000; Abcam ab8822), mouse anti-human CD27 (1:100; Biolegend 356403), mouse anti-human CD20 (1:100; eBioScience 14-0202-82), mouse anti-human IgD (af647-conjugated, 1:50 or 1:100; Biolegend 348227), rabbit anti-HSV2 (1:1000, Dako B0116), mouse anti-CD4 (1:1000, Biolegend 300502), and mouse anti-CD8 (af647-conjugated, 1:100, BD Pharmingen 557708). Prior to application of antibodies, non-specific binding was blocked with 2% bovine serum albumin, 10% casein, and 5% normal human sera, except for mouse-anti-human IgG and IgD, where human sera were omitted from the blocking buffer. TSA amplification (Invitrogen) was used for visualization of CD79b and IgG, and for CD20 in co-staining with IgD. Tissue sections were mounted in Mowiol 40-88 containing 2.5% w/v DABCO (Sigma-Aldrich). Images were captured with Nikon Eclipse Ti with NIS-Elements Software using a Hamamatsu ORCA-Flash 4.0 sCMOS camera and viewed in ImageJ/FIJI (60). Cells were counted in ImageJ/FIJI with the cell counter plugin (61). The surface area of each biopsy was calculated in ImageJ.

Fluorescent in situ hybridization (FISH): To identify the presence of IgG-producing cells in biopsies and identify their spatial localization and interaction with other cell types, we performed FISH (RNAscope®2.0, ACDBio) (62). Freshly sliced, 8 μm frozen tissue sections were fixed at 4°C in 10% neutral buffered formalin, dehydrated, and treated with protease. Prepared sections were incubated with DNA-based probes (ACDBio) for pooled *IGHG1-4* (IgG), *CD4*, *MS4A1* (CD20), *SDC1* (CD138), *PAX5*, *CXCR4*, *PRDM1* and *IRF4* transcripts, and fluorescently labeled for visualization. After nuclear staining with DAPI (Fluka), tissues were mounted with

ProLong Gold Antifade (Thermo Fisher). Images were captured with Nikon Eclipse Ti (as above) and viewed in ImageJ/FIJI. IgG RNA^+ positive cells were counted manually over the entire slice and the surface area of each biopsy slice was calculated in ImageJ (61) to determine B-cell density. Some sections were then unmounted and stained by IF for vWF (Abcam) to determine the relative localization of B cells identified by FISH with respect to small capillaries. Colocalization of CD138 and IgG FISH probes was investigated by deconvolution (GEA/Applied Precision DeltaVision Elite) and confocal (Zeiss LSM 780 NLO) microscopy at 60x magnification, confocal and deconvolution images were taken with a high-resolution cooled Photometrics HQ2 CCD camera.

Preparation of biopsy extract: Five or ten freshly sliced, 10 μm biopsy cryosections were placed in a microcentrifuge tube on dry ice. To extract protein, tubes were brought to room temperature and Tissue Extraction Reagent II (Invitrogen) was added (10 μl per biopsy slice). Tube content was pipetted to mix followed by sequential vortexing (30 sec), sonication (30 sec) and pulse centrifugation. This procedure was repeated twice, then samples were flash frozen on dry ice and kept until use at –20°C. Upon thawing, samples were vortexed, sonicated and centrifuged for 5 min at 14500 x g. The supernatant was collected to measure protein, total IgG and HSV-specific antibodies via Luminex binding antibody assay.

HSV2 Luminex binding antibody assay: HSV2 proteins (gB2, gD2) and control antigens (EBV gp350, Flu-HA) were coupled to MagPlex beads using an antibody coupling kit (Luminex Corp.) and stored at 4°C. To measure HSV2 specific antibody, MagPlex beads were incubated with

blocking buffer (5% Blotting-Grade Blocker (Bio-Rad), 0.05% Tween-20 (Sigma), phosphate buffered saline (PBS)) to minimize non-specific binding. Beads were then washed and mixed with serial dilutions of biopsy extracts or serum samples in assay buffer (Pierce™ Protein-Free (PBS) Blocking Buffer, 1% Blotting-Grade Blocker, and 0.05% Tween-20). Sera pooled from ten HSV2 seropositive and ten HSV2 seronegative donors were used as positive and negative controls, respectively. After incubation with biopsy extracts or serum samples, MagPlex beads were washed with PBST (PBS, 0.05% Tween-20) and incubated with anti-human IgG Fc-PE (Southern Biotech). Finally, beads were washed 3 times and resuspended in PBS containing 1% BSA and 0.05% Tween-20. Median fluorescence intensity (MFI) by PE fluorescence for each bead type was collected on Luminex 200 instruments (Luminex Corp.) operated by MagPlex software (Hitachi) or xPonent Software (Luminex Corp.). The level of background was assigned by the MFI of antigen-conjugated beads incubated first with buffer (in place of serum), then with secondary antibody. Background MFI values for each antigen were subtracted from experimental measurements. The MFI value of the biopsy extracts was normalized to the surface area of each biopsy slice (as measured in adjacent slices) to account for variation in size and protein composition of biopsy specimens. Values from the dilution curves were used to determine the area under the curve (AUC). Serologic data were analyzed in GraphPad Prism.

HSV2 quantitative PCR: DNA from biopsies and genital swabs was extracted using tissue kits (EZ1; QIAGEN) from 60–80 µm cross-sectioned samples from each biopsy specimen as previously described (63, 64), including subtype-specific typing by real-time PCR (65). HSV2 DNA copy numbers were normalized to $1x10^6$ cells using β-globin copy numbers. Primers used were

5′-TGAAGGCTCATGGCAAGAAA-3′ and 5′-GCTCACTCAGTGTGGCAAAGG-3′ with 5′-TCCAGGTGAGCCAGGCCATCACTA-3′ as a probe. Detection limits of HSV2 DNA quantification were one copy per 50,000 cells in tissue, as previously published (50, 63).

Statistics: All statistics and data analysis were performed using R Studio (R 3.4.1, R Core Team, Vienna, Austria) or GraphPad Prism version 8.2.0 for Mac (GraphPad Software, California, USA). To compare cell density and antibody concentration between biopsy time points the Friedman test with Dunn's correction for multiple comparisons was used. To test the observation of greatest B cell and ASC density the maximum of lesion or newly healed was compared to the maximum at 2, 4 or 8 weeks after healing by a paired Wilcoxon test. We employed repeated measures correlation to account for the presence of multiple biopsies from each participant (66). The repeated measures correlation coefficient between the density of cell types (r) and statistical test value (p) is shown on the scatter plot. To avoid taking log of zero, a small pseudo count (50% of the lowest value) was added to each measurement prior to log transformation. Comparison of AUC calculated for sera collected at different time points was performed with the Friedman test with Dunn's correction for multiple comparisons. Statistical significance was defined as adjusted, two-sided p value ≤ 0.05.

Study approval: The natural history biopsy protocol was approved by the University of Washington Institutional Review Board (IRB) and written, informed consent was obtained from each participant.

Author contributions:
Study design: ESF, AMS, JZ, LC
Tissue biopsy analysis: ESF, AMS, AK, KP, RMB, SSC
Participant recruitment and clinical guidance: CJ, AW
Data analysis: ESF, AMS, RMB, JS, RR, PTE, JZ, TP
Manuscript preparation: ESF, AMS, JZ, LC
All authors reviewed and approved of the manuscript.
ESF is listed first as co-first author due to contribution to the revision of the manuscript, ESF and AMS contributed equally to the design and undertaking of experiments and the analysis presented here.

Acknowledgements:
The authors would like to express their appreciation to Mindy Miner for her assistance in editing and formatting the final manuscript and to David McDonald for assistance in confocal and deconvolution microscopy.

References
1. Wald A, Zeh J, Selke S, Ashley RL, Corey L. Virologic characteristics of subclinical and symptomatic genital herpes infections. *N. Engl. J. Med.* 1995;333(12):770–775.
2. Benedetti J, Corey L, Ashley R. Recurrence rates in genital herpes after symptomatic first-episode infection. *Ann. Intern. Med.* 1994;121(11):847–854.
3. Schiffer JT et al. Mathematical modeling predicts that increased HSV-2 shedding in HIV-1 infected persons is due to poor immunologic control in ganglia and genital mucosa. *PLoS One* 2016;11(6):e0155124.
4. Schiffer JT et al. Mucosal host immune response predicts the severity and duration of herpes simplex virus-2 genital tract shedding episodes. *Proc. Natl. Acad. Sci. U. S. A.* 2010;107(44):18973–18978.
5. Zhu J et al. Virus-specific CD8+ T cells accumulate near sensory nerve endings in genital skin during subclinical HSV-2 reactivation. *J. Exp. Med.* 2007;204(3):595–603.
6. Iijima N et al. Dendritic cells and B cells maximize mucosal Th1 memory response to herpes simplex virus. *J. Exp. Med.* 2008;205(13):3041–3052.
7. Zhu J et al. Persistence of HIV-1 receptor-positive cells after HSV-2 reactivation is a potential mechanism for increased HIV-1 acquisition. *Nat. Med.* 2009;15(8):886–892.
8. Zhu J et al. Immune surveillance by CD8αα+ skin-resident T cells in human herpes virus infection. *Nature* 2013;497(7450):494–7.
9. Schiffer JT et al. Rapid localized spread and immunologic containment define Herpes simplex virus-2 reactivation in the human genital tract. *Elife* 2013;2:e00288.
10. Iijima N, Iwasaki A. A local macrophage chemokine network sustains protective tissue-resident memory CD4 T cells. *Science.* 2014;346(6205):93–98.
11. Mertz GJ et al. Frequency of acquisition of first-episode genital infection with herpes simplex virus from symptomatic and asymptomatic source contacts. *Sex. Transm. Dis.* 1985;12(1):33–9.
12. Cairns TM et al. Dissection of the antibody response against herpes simplex virus glycoproteins in naturally infected humans. *J. Virol.* 2014;88(21):12612–12622.

13. Flechtner JB et al. Immune responses elicited by the GEN-003 candidate HSV-2 therapeutic vaccine in a randomized controlled dose-ranging phase 1/2a trial. *Vaccine* 2016;34(44):5314–5320.
14. Bernstein DI et al. Therapeutic vaccine for genital herpes simplex virus-2 infection: Findings from a randomized trial. *J. Infect. Dis.* 2017;215(6):856–864.
15. Wald A et al. Therapeutic HSV-2 vaccine (GEN003) results in durable reduction in genital lesions at 1 year. *Open Forum Infect. Dis.* 2014;1(Suppl 1):S55–S56.
16. Gilbert PB et al. Antibody to HSV gD peptide induced by vaccination does not protect against HSV-2 infection in HSV-2 seronegative women. *PLoS One* 2017;12(5):e0176428.
17. Burn C et al. An HSV-2 single-cycle candidate vaccine deleted in glycoprotein D, ΔgD-2, protects male mice from lethal skin challenge with clinical isolates of HSV-1 and HSV-2. *J. Infect. Dis.* 2017;217(5):754–758.
18. Jiang Y et al. Maternal antiviral immunoglobulin accumulates in neural tissue of neonates to prevent HSV neurological disease. *MBio* 2017;8(4):1–14.
19. Criscuolo E et al. Cell-to-cell spread-blocking activity is extremely limited in the sera of HSV-1 and HSV-2 infected subjects. *J. Virol.* 2019;93:e00070-19.
20. Harandi AM, Svennerholm B, Holmgren J, Eriksson K. Differential roles of B cells and IFN-γ-secreting CD4+ T cells in innate and adaptive immune control of genital herpes simplex virus type 2 infection in mice. *J. Gen. Virol.* 2001;82(4):845–853.
21. Dudley KL, Bourne N, Milligan GN. Immune protection against HSV-2 in B-cell-deficient mice. *Virology* 2000;270(2):454–463.
22. Milligan GN, Bernstein DI. Generation of humoral immune responses against herpes simplex virus type 2 in the murine female genital tract. *Virology* 1995;206(1):234–41.
23. Bourne N et al. Increased frequency of virus shedding by herpes simplex virus 2-infected guinea pigs in the absence of CD4 + T lymphocytes. *J. Virol.* 2018;93(4):e01721-18.
24. Oh JE et al. Migrant memory B cells secrete luminal antibody in the vagina. *Nature* 2019;571:122–126.
25. Mandal A et al. Cell and fluid sampling microneedle patches for monitoring skin-resident immunity. *Sci. Transl. Med.* 2018;10(467):eaar2227.
26. Tabib T, Morse C, Wang T, Chen W, Lafyatis R. SFRP2/DPP4 and FMO1/LSP1 define major fibroblast populations in human skin. *J. Invest. Dermatol.* 2018;138(4):802–810.
27. Lemos MP et al. In men at risk of HIV infection, IgM, IgG1, IgG3, and IgA reach the human foreskin epidermis. *Mucosal Immunol.* 2016;9(3):798–808.
28. Cunningham AL, Turner RR, Miller AC, Para MF, Merigan TC. Evolution of recurrent herpes simplex lesions: an immunohistologic study. *J. Clin. Invest.* 1985;75(1):226–233.
29. Egbuniwe IU, Karagiannis SN, Nestle FO, Lacy KE. Revisiting the role of B cells in skin immune surveillance. *Trends Immunol.* 2015;36(2):102–111.
30. Geherin S a et al. The skin, a novel niche for recirculating B cells. *J. Immunol.* 2012;188(12):6027–6035.
31. Ginaldi L, De Martinis M, D'Ostilio A, Marini L, Quaglino D. Changes in antigen expression on B lymphocytes during HIV infection. *Pathobiology* 1998;66(1):17–23.
32. Wilson RP et al. IgM plasma cells reside in healthy skin and accumulate with chronic inflammation. *J. Invest. Dermatol.* 2019;139(12):2477–2487.
33. Stevens RH, Askonas BA, Welstead JL. Immunoglobulin heavy chain mRNA in mitogen-

stimulate B cells. *Eur. J. Immunol.* 1975;5(1):47–53.
34. Coronella JA, Telleman P, Truong TD, Ylera F, Junghans RP. Amplification of IgG VH and VL (Fab) from single human plasma cells and B cells. *Nucleic Acids Res.* 2000;28(20):e85.
35. Nutt SL, Hodgkin PD, Tarlinton DM, Corcoran LM. The generation of antibody-secreting plasma cells. *Nat. Rev. Immunol.* 2015;15(3):160–171.
36. Tellier J et al. Blimp-1 controls plasma cell function through the regulation of immunoglobulin secretion and the unfolded protein response. *Nat. Immunol.* 2016;17(3):323–330.
37. Nutt SL, Taubenheim N, Hasbold J, Corcoran LM, Hodgkin PD. The genetic network controlling plasma cell differentiation. *Semin. Immunol.* 2011;23(5):341–349.
38. Ellebedy AH et al. Defining antigen-specific plasmablast and memory B cell subsets in human blood after viral infection or vaccination. *Nat. Immunol.* 2016;17(10):1226–1234.
39. Minnich M et al. Multifunctional role of the transcription factor Blimp-1 in coordinating plasma cell differentiation. *Nat. Immunol.* 2016;17(3):331–343.
40. Chilosi M et al. CD138/syndecan-1: A useful immunohistochemical marker of normal and neoplastic plasma cells on routine trephine bone marrow biopsies. *Mod. Pathol.* 1999;12(12):1101–1106.
41. O'Connell FP, Pinkus JL, Pinkus GS. CD138 (Syndecan-1), a plasma cell marker immunohistochemical profile in hematopoietic and nonhematopoietic neoplasms. *Am. J. Clin. Pathol.* 2004;121(2):254–263.
42. Kind S et al. Prevalence of Syndecan-1 (CD138) Expression in Different Kinds of Human Tumors and Normal Tissues. *Dis. Markers* 2019;2019:4928315.
43. Bugatti S, Vitolo B, Caporali R, Montecucco C, Manzo A. B Cells in Rheumatoid Arthritis: From Pathogenic Players to Disease Biomarkers. *Biomed Res. Int.* 2014;681678:1–14.
44. Hauser AE et al. Chemotactic responsiveness toward ligands for CXCR3 and CXCR4 is regulated on plasma blasts during the time course of a memory immune response. *J. Immunol.* 2002;169(3):1277–1282.
45. Nie Y et al. The role of CXCR4 in maintaining peripheral B cell compartments and humoral immunity. *J. Exp. Med.* 2004;200(9):1145–1156.
46. Caraux A et al. Circulating human B and plasma cells. Age-associated changes in counts and detailed characterization of circulating normal CD138- and CD138+ plasma cells. *Haematologica* 2010;95(6):1016–1020.
47. Nance CL, Shearer WT. SDF-1α regulates HIV-1-gp120-induced changes in CD79b surface expression and Ig production in activated human B cells. *Clin. Immunol.* 2002;105(2):208–214.
48. Peng T et al. Evasion of the mucosal innate immune system by herpes simplex virus type 2. *J. Virol.* 2009;83(23):12559–12568.
49. Hensel MT et al. Selective expression of CCR10 and CXCR3 by circulating human herpes simplex virus-specific CD8 T cells. *J. Virol.* 2017;91(19):e00810-17.
50. Peng T et al. An effector phenotype of CD8+ T cells at the junction epithelium during clinical quiescence of herpes simplex virus 2 infection. *J. Virol.* 2012;86(19):10587–10596.
51. Douglas RG, Couch RB. A prospective study of chronic herpes simplex virus infection and recurrent herpes labialis in humans. *J. Immunol.* 1970;2:289–295.
52. Friedman MG, Kimmel N. Herpes simplex virus-specific serum immunoglobulin A: Detection in patients with primary or recurrent herpes infections and in healthy adults. *Infect. Immun.*

1982;37(1):374–377.
53. Juto P, Settergren B. Specific serum IgA, IgG and IgM antibody determination by a modified indirect ELISA-technique in primary and recurrent herpes simplex virus infection. *J. Virol. Methods* 1988;20(1):45–55.
54. Woodman CB et al. The relative infrequency and low levels of neutralising and immunoprecipitating antibody to herpes simplex viruses types 1 and 2 in patients with a history of recurrent herpes genitalis. *Med. Microbiol. Immunol.* 1983;171(4):243–250.
55. Griss J et al. B cells sustain inflammation and predict response to immune checkpoint blockade in human melanoma. *Nat. Commun.* 2019;10(1):4186.
56. Blanchard-Rohner G, Pulickal AS, Jol-van Der Zijde CM, Snape MD, Pollard AJ. Appearance of peripheral blood plasma cells and memory B cells in a primary and secondary immune response in humans. *Blood* 2009;114(24):4998–5002.
57. He XS et al. Plasmablast-derived polyclonal antibody response after influenza vaccination. *J. Immunol. Methods* 2011;365(1–2):67–75.
58. Ashley RL, Militoni J, Lee F, Nahmias A, Corey L. Comparison of Western blot (immunoblot) and glycoprotein G-specific immunodot enzyme assay for detecting antibodies to herpes simplex virus types 1 and 2 in human sera. *J. Clin. Microbiol.* 1988;26(4):662–667.
59. Lingwood D et al. Structural and genetic basis for development of broadly neutralizing influenza antibodies. *Nature* 2012;489(7417):566–570.
60. Schindelin J et al. Fiji: An open-source platform for biological-image analysis. *Nat. Methods* 2012;9(7):676–682.
61. Diem K et al. Image analysis for accurately counting CD4+ and CD8+ T cells in human tissue. *J. Virol. Methods* 2015;222:117–121.
62. Wang F et al. RNAscope: A novel in situ RNA analysis platform for formalin-fixed, paraffin-embedded tissues. *J. Mol. Diagnostics* 2012;14(1):22–29.
63. Magaret AS, Wald A, Huang M-L, Selke S, Corey L. Optimizing PCR positivity criterion for detection of herpes simplex virus DNA on skin and mucosa. *J. Clin. Microbiol.* 2007;45(5):1618–1620.
64. Wald A, Huang M-L, Carrell D, Selke S, Corey L. Polymerase chain reaction for detection of herpes simplex virus (HSV) DNA on mucosal surfaces: comparison with HSV isolation in cell culture. *J. Infect. Dis.* 2003;188(9):1345–51.
65. Corey L, Huang M-L, Selke S, Wald A. Differentiation of herpes simplex virus types 1 and 2 in clinical samples by a real-time taqman PCR assay. *J. Med. Virol.* 2005;76:350–355.
66. Bakdash JZ, Marusich LR. Repeated measures correlation. *Front. Psychol.* 2017;8:1–13.

Figure 1. **Antigen-naïve CD20$^+$ B cells and IgG RNA$^+$ cells infiltrate lesion-area skin during HSV2 reactivation but not uninvolved skin.** (**A**) B cells: CD20 (red) and CD79b (green) in serial genital skin biopsies during and after HSV2 lesion from a single person (shown 1/10 persons). Scale bars are 100 μm. There were no B cells detected in the control biopsy. (**B**) T cells: CD4 (green) and CD8 (red) in serial biopsies during and after HSV2 reactivation (shown 1/8 persons). (**C**) Densely clustered CD4$^+$CD8$^+$ T cells (left) in this person were accompanied by CD20$^+$CD79b$^+$ B cells (right); scale bar is 50 μm. (**D**) CD27 (green) and CD20 (red) from a lesion biopsy with no evidence of co-staining (shown 1/6 persons); scale bar is 50 μm. (**E**) In a healing skin biopsy, B cells express CD20 (green) and IgD (red), (shown 1/5 persons). Inset shows red and green channels separately. Scale bar is 50 μm. (**F**) IgG-producing cells are loaded with IgG RNA by FISH. IgG mRNA (green) in a healing biopsy of HSV2 reactivation (shown 1/9 persons). 40x magnification by oil immersion. Scale bar is 25 μm. (**G**) IgG$^+$ cells by FISH over time showing distribution within the upper dermis and lymphocyte clusters. In this person the control biopsy (from the arm) had no IgG$^+$ cells. Dashed line indicates the DEJ. Images obtained at 20x, scale bars are 250 μm. Brightness in G was increased for consistency.

Figure 2. Cells expressing a high level of IgG RNA infiltrate genital skin during the tissue-based immune response to HSV2 reactivation. (**A**) A healing lesion shows *PRDM1* (Blimp-1) expression in many IgG RNA$^+$ cells (40x immersion lens, scale bar 25 μm). Scale bar is 25μm. Shown 1/5 persons. Brightness increased for visualization (**B**) IgG-producing cells by FISH. IgG mRNA (red) and IRF4 (green) in a healing biopsy of HSV2 reactivation. Note two cells with lower amplitude of IgG that are IRF4-. Image is 60x by confocal microscopy. (Scale bar 25 μm, shown

1/7 persons). (**C**) IgG RNA (red) and CD20 RNA (green) adjacent cells without co-expression. Image is 40x by oil immersion microscopy, scale bar is 25 μm. Shown 1/5 persons. (**D**) IgG (green) and CD138 (red) co-expression by deconvolution microscopy (60x, single Z stack image shown) 8 of 20 IgG RNA^+ cells in this image also express CD138. Insets are single color images of center cells. Shown 1/4 persons. (**E**) *PAX5* (red) and high levels of IgG RNA (green) were not observed to co-express, whereas *PAX5* and CD20 RNA were. Image is 40x by oil immersion microscopy, scale bars are 25 μm, shown 1/5 persons. (**F**). An active lesion shows two cells with co-expression of CXCR4 and IgG (40x immersion lens, scale bar 25 μm). Shown 1/3 persons.

Figure 3. IgG RNA+ cells in relation to other tissue structures and cell types. (**A**) Antibody-secreting cells are found infiltrating tissue distant from vascular structures, as well as adjacent to and within small capillaries. IgG-producing cells identified by FISH in a healing biopsy are found independently in tissue (left) as well as proximate to small capillaries (right) in biopsies from healing HSV2 reactivation. Faint green signal is due to collagen autofluorescence. Blood vessel endothelial cells identified by vWF IF (green), IgG RNA^+ cells (magenta). Scale bar in large image is 200 μm, bars in insets are 25 μm. vWF and IgG colocalization by combination FISH and IF was performed in biopsies from 6 persons. While capillaries were identified in all biopsies, IgG cells were not present within these vascular structures in all biopsies. (**B**) IgG-producing cells by FISH (left) clustered in area of dense T-cell infiltration (right): CD4 (green) and CD8 (red), shown are serial sections of the same biopsy. Scale bar is 50 μm. IgG FISH and T-cell IF was performed in serial biopsies from 4 persons. (**C**) Clustered IgG (red) and CD4 (green) by

FISH, absence of vWF staining was confirmed. Scale bar is 50 µm. IgG and CD4 FISH was performed in biopsies from 8 persons.

Figure 4. Migration kinetics of B and T cells into genital skin during HSV2 reactivation and tissue healing by type of biopsy (left) and over time (right). Density of (**A**) $CD20^+$ cells by IF (n=11), (**B**) IgG RNA^+ cells by FISH (n=10), (**C**) $CD4^+$ T cells by IF (n=8) and (**D**) $CD8^+$ T cells by IF (n=8) in tissue over time and shown by persons with cell density peak at lesion (middle) or healing (right) time points. Statistical testing is by Friedman test with Dunn's corrections for multiple comparisons. Each graph on the right presents cell counts from genital area biopsies over time, as measured from the identified symptomatic lesion. (**E**) Correlation (r) between B and T cell subsets and between $CD20^+$ and IgG RNA^+ cells was calculated by repeated measures correlation. Participants are labeled by color, multiple biopsies from genital and control areas from each participant are included in each graph.

Figure 5. Antibody is detectable during the tissue-based immune response to HSV2 reactivation and the amount is variable over time. (**A**) Immunofluorescent detection of IgG (green) in genital skin biopsies in one subject. Scale bar represents 250 µm. Brightness increased for visualization, shown 1/10 persons. (**B**) Spatial localization of in-tissue IgG vs HSV antigen by IF in biopsy of an active HSV2 lesion (different subject). Antigen is seen in multiple locations with the highest density of IgG at the site of vesicle formation. Scale bar is 250µm. The distribution of IgG and HSV antigen across multiple sites of viral involvement was unique to this biopsy.

Figure 6. Levels of HSV2 specific antibody and total IgG follow B-cell and ASC density.

Concentration (expressed as MFI normalized to biopsy surface area (mm^2)) of IgG to (**A**) gB2, (**B**) gD2 (n=14), (**C**) total IgG (measured in ng/mm^2, n=13), and (**D**) control antigens EBV-gp350 and Flu-HA (n=6) in tissue over time and shown by persons with antibody peak at lesion (1^{st} column) or healing (2^{nd} and 3^{rd} column) time points. If a person did not have a clear peak at one time point, they were included in multiple graphs. Levels of antibody over time (by number of days after lesion biopsy) is in the 4^{th} column. Missing data points (such as the arm control in person 6) correspond to biopsies with insufficient tissue to run the test. (**E**) The area under the titration curve in a serum measurement of antibody specific to each of these antigens from a single sample taken from each person at study entry (n=15). Serum titration curves are in Supplementary Figure 4 and AUC values are in the Supplementary Table 2. Statistical testing is by Friedman test with Dunn's corrections for multiple comparisons. All measurements are performed in duplicate.

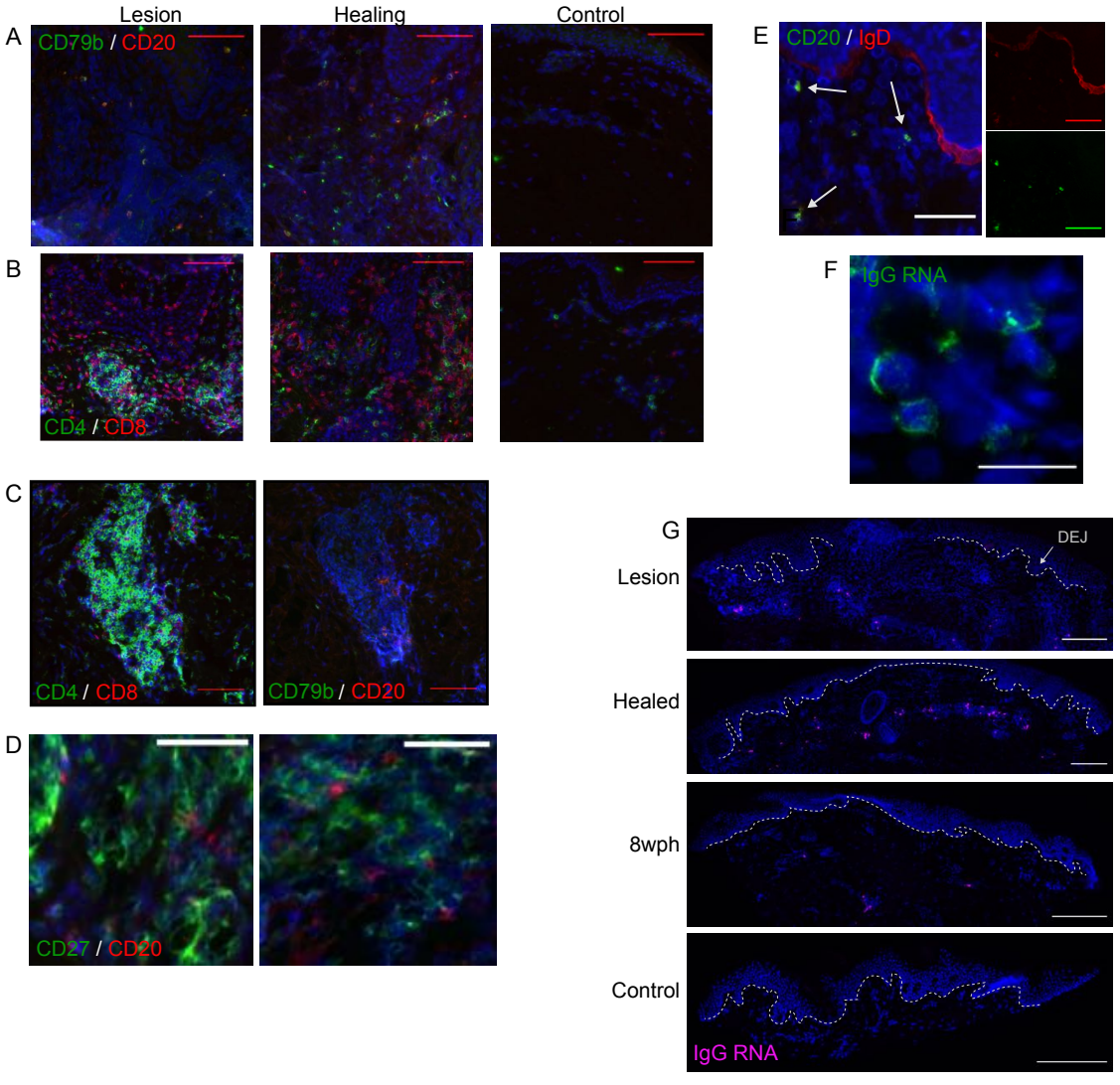

Figure 1. Antigen-naïve CD20+ B cells and IgG RNA+ cells infiltrate lesion-area skin during HSV2 reactivation but not uninvolved skin. (A) B cells: CD20 (red) and CD79b (green) in serial genital skin biopsies during and after HSV2 lesion from a single person (shown 1/10 persons). Scale bars are 100 μm. There were no B cells detected in the control biopsy. (B) T cells: CD4 (green) and CD8 (red) in serial biopsies during and after HSV2 reactivation (shown 1/8 persons). (C) Densely clustered CD4+CD8+ T cells (left) in this person were accompanied by CD20+CD79b+ B cells (right); scale bar is 50 μm. (D) CD27 (green) and CD20 (red) from a lesion biopsy with no evidence of co-staining (shown 1/6 persons); scale bar is 50 μm. (E) In a healing skin biopsy, B cells express CD20 (green) and IgD (red), (shown 1/5 persons). Inset shows red and green channels separately. Scale bar is 50 μm. (F) IgG-producing cells are loaded with IgG RNA by FISH. IgG mRNA (green) in a healing biopsy of HSV2 reactivation (shown 1/9 persons). 40x magnification by oil immersion. Scale bar is 25 μm. (G) IgG+ cells by FISH over time showing distribution within the upper dermis and lymphocyte clusters. In this person the control biopsy (from the arm) had no IgG+ cells. Dashed line indicates the DEJ. Images obtained at 20x, scale bars are 250 μm. Brightness in G was increased for consistency.

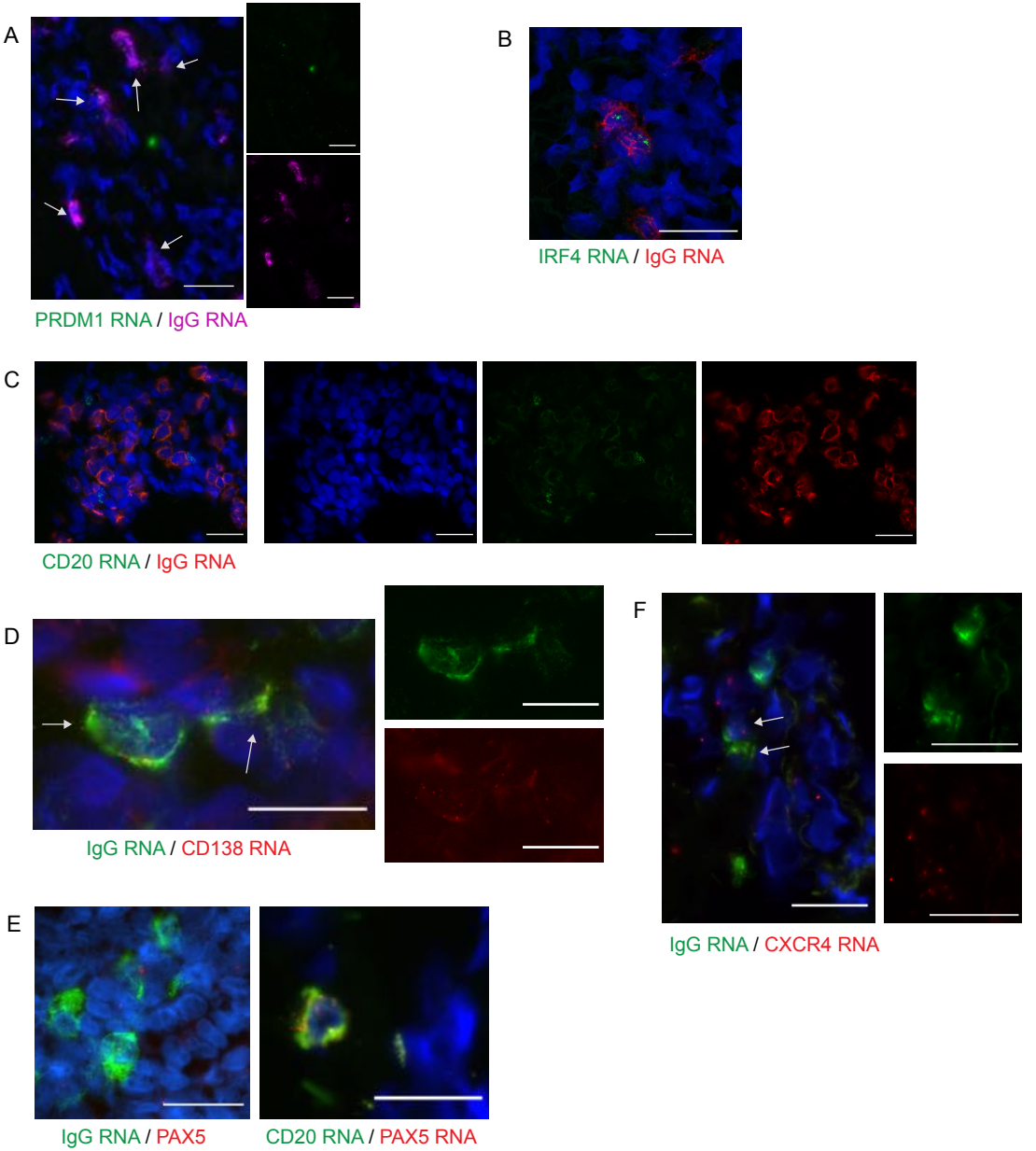

Figure 2. Cells expressing a high level of IgG RNA infiltrate genital skin during the tissue-based immune response to HSV2 reactivation. (A) A healing lesion shows PRDM1 (Blimp-1) expression in many IgG RNA+ cells (40x immersion lens, scale bar 25 µm). Scale bar is 25µm. Shown 1/5 persons. Brightness increased for visualization (B) IgG-producing cells by FISH. IgG mRNA (red) and IRF4 (green) in a healing biopsy of HSV2 reactivation. Note two cells with lower amplitude of IgG that are IRF4-. Image is 60x by confocal microscopy. (Scale bar 25 µm, shown 1/7 persons). (C) IgG RNA (red) and CD20 RNA (green) adjacent cells without co-expression. Image is 40x by oil immersion microscopy, scale bar is 25 µm. Shown 1/5 persons. (D) IgG (green) and CD138 (red) co-expression by deconvolution microscopy (60x, single Z stack image shown) 8 of 20 IgG RNA+ cells in this image also express CD138. Insets are single color images of center cells. Shown 1/4 persons. (E) PAX5 (red) and high levels of IgG RNA (green) were not observed to co-express, whereas PAX5 and CD20 RNA were. Image is 40x by oil immersion microscopy, scale bars are 25 µm, shown 1/5 persons. (F). An active lesion shows two cells with co-expression of CXCR4 and IgG (40x immersion lens, scale bar 25 µm). Shown 1/3 persons.

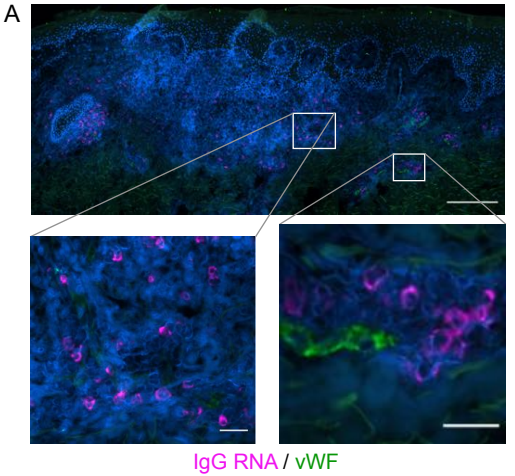

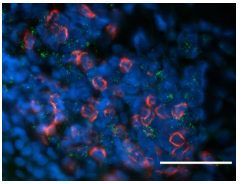

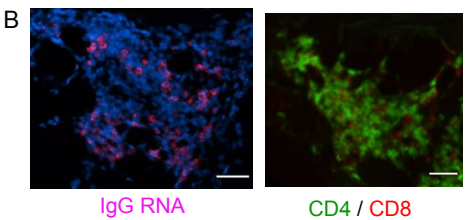

Figure 3. IgG RNA+ cells in relation to other tissue structures and cell types. (A) Antibody-secreting cells are found infiltrating tissue distant from vascular structures, as well as adjacent to and within small capillaries. IgG-producing cells identified by FISH in a healing biopsy are found independently in tissue (left) as well as proximate to small capillaries (right) in biopsies from healing HSV2 reactivation. Faint green signal is due to collagen autofluorescence. Blood vessel endothelial cells identified by vWF IF (green), IgG RNA+ cells (magenta). Scale bar in large image is 200 μm, bars in insets are 25 μm. vWF and IgG colocalization by combination FISH and IF was performed in biopsies from 6 persons. While capillaries were identified in all biopsies, IgG cells were not present within these vascular structures in all biopsies. (B) IgG-producing cells by FISH (left) clustered in area of dense T-cell infiltration (right): CD4 (green) and CD8 (red), shown are serial sections of the same biopsy. Scale bar is 50 μm. IgG FISH and T-cell IF was performed in serial biopsies from 4 persons. (C) Clustered IgG (red) and CD4 (green) by FISH, absence of vWF staining was confirmed. Scale bar is 50 μm. IgG and CD4 FISH was performed in biopsies from 8 persons.

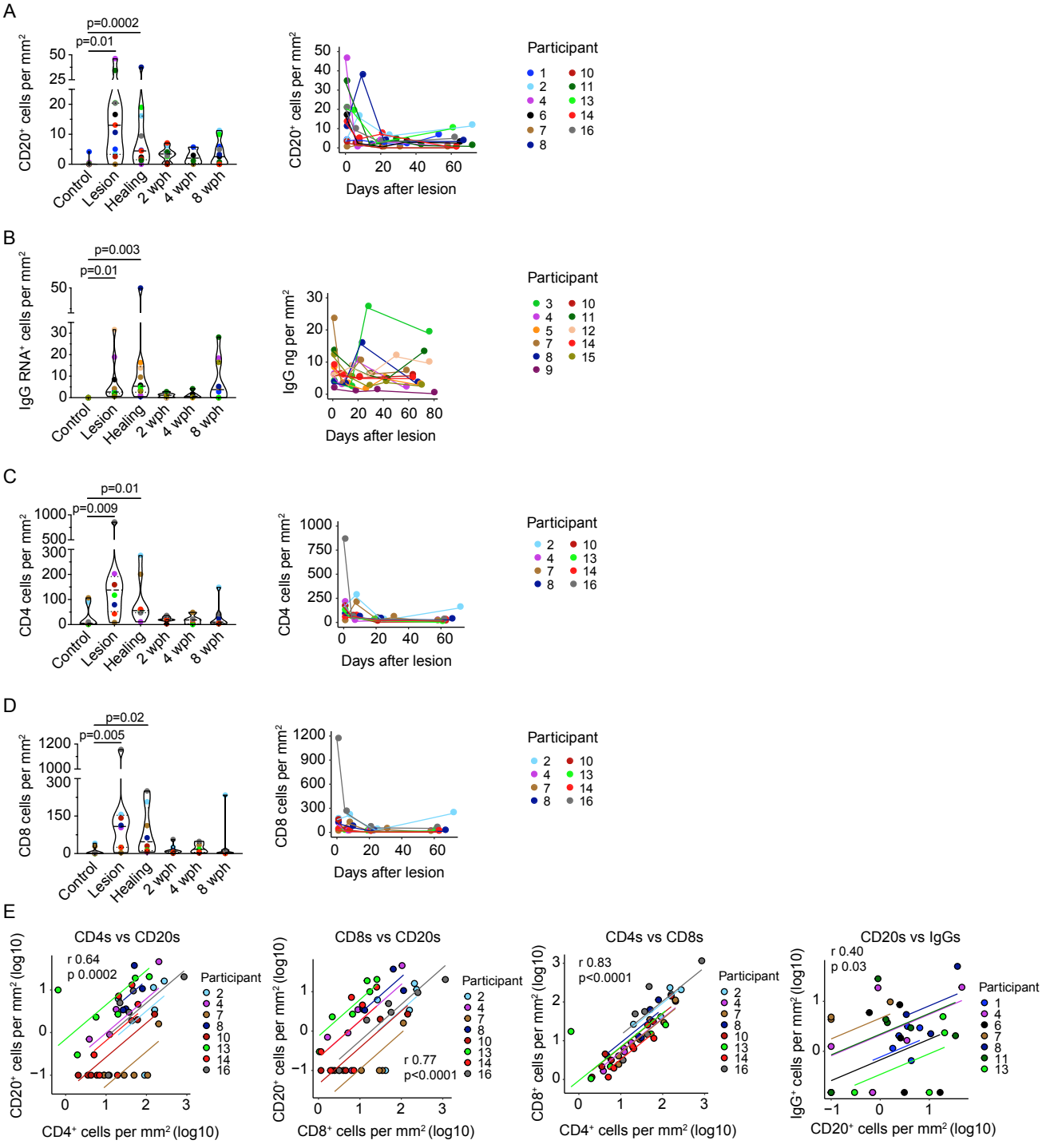

Figure 4. Migration kinetics of B and T cells into genital skin during HSV2 reactivation and tissue healing by type of biopsy (left) and over time (right). Density of (A) CD20+ cells by IF (n=11), (B) IgG RNA+ cells by FISH (n=10), (C) CD4+ T cells by IF (n=8) and (D) CD8+ T cells by IF (n=8) in tissue over time and shown by persons with cell density peak at lesion (middle) or healing (right) time points. Statistical testing is by Friedman test with Dunn's corrections for multiple comparisons. Each graph on the right presents cell counts from genital area biopsies over time, as measured from the identified symptomatic lesion. (E) Correlation (r) between B and T cell subsets and between CD20+ and IgG RNA+ cells was calculated by repeated measures correlation. Participants are labeled by color, multiple biopsies from genital and control areas from each participant are included in each graph.

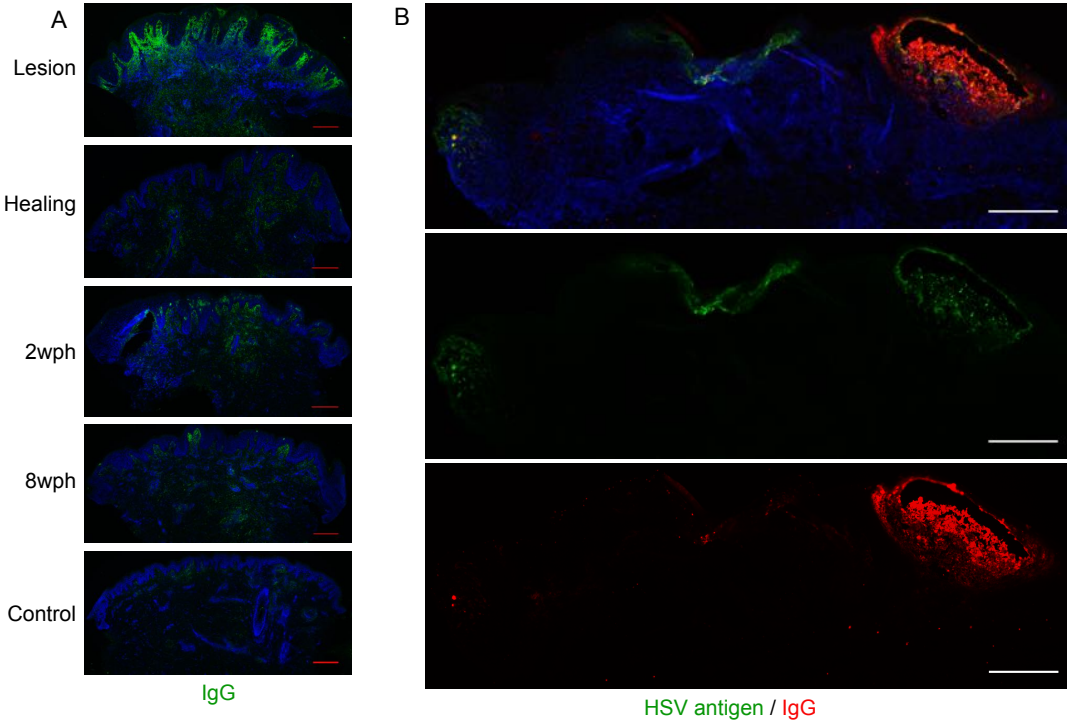

Figure 5. Antibody is detectable during the tissue-based immune response to HSV2 reactivation and the amount is variable over time. (A) Immunofluorescent detection of IgG (green) in genital skin biopsies in one subject. Scale bar represents 250 μm. Brightness increased for visualization, shown 1/10 persons. (B) Spatial localization of in-tissue IgG vs HSV antigen by IF in biopsy of an active HSV2 lesion (different subject). Antigen is seen in multiple locations with the highest density of IgG at the site of vesicle formation. Scale bar is 250μm. The distribution of IgG and HSV antigen across multiple sites of viral involvement was unique to this biopsy.

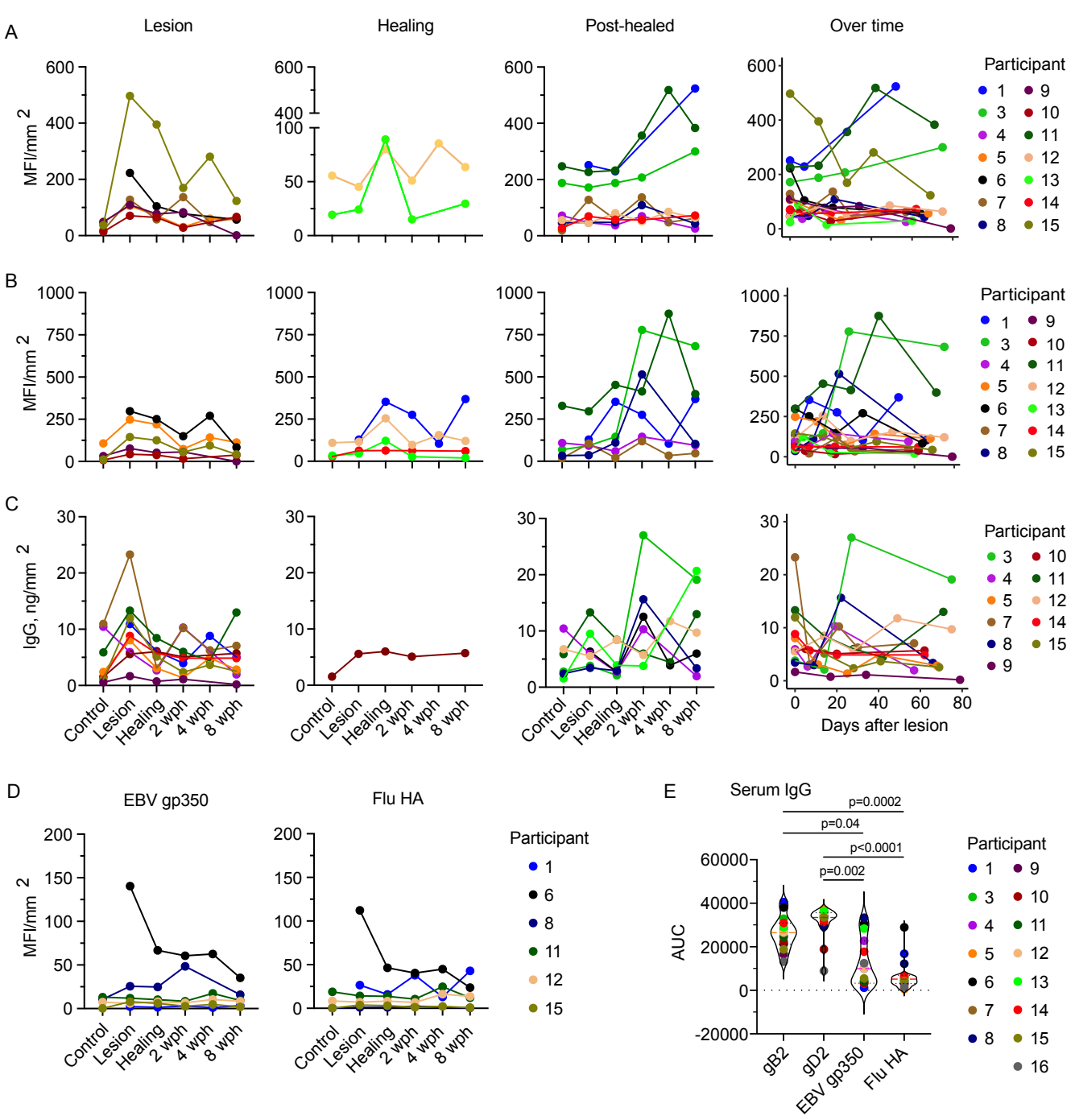

Figure 6. Levels of HSV2 specific antibody and total IgG follow B-cell and ASC density. Concentration (expressed as MFI normalized to biopsy surface area (mm2)) of IgG to (A) gB2, (B) gD2 (n=14), (C) total IgG (measured in ng/mm2, n=13), and (D) control antigens EBV-gp350 and Flu-HA (n=6) in tissue over time and shown by persons with antibody peak at lesion (1st column) or healing (2nd and 3rd column) time points. If a person did not have a clear peak at one time point, they were included in multiple graphs. Levels of antibody over time (by number of days after lesion biopsy) is in the 4th column. Missing data points (such as the arm control in person 6) correspond to biopsies with insufficient tissue to run the test. (E) The area under the titration curve in a serum measurement of antibody specific to each of these antigens from a single sample taken from each person at study entry (n=15). Serum titration curves are in Supplementary Figure 4 and AUC values are in the Supplementary Table 2. Statistical testing is by Friedman test with Dunn's corrections for multiple comparisons. All measurements are performed in duplicate.